Journal of Membrane Science 538 (2017) 86–95

Contents lists available at ScienceDirect

Journal of Membrane Science

journal homepage: www.elsevier.com/locate/memsci

Nanocomposite membranes based on alginate matrix and high loading of pegylated POSS for pervaporation dehydration

Manru Wang[a,b], Ruisi Xing[a,b], Hong Wu[a,b,c,*], Fusheng Pan[a,b], Junjie Zhang[a,b], He Ding[a,b], Zhongyi Jiang[a,b]

[a] Key Laboratory for Green Chemical Technology of Ministry of Education, School of Chemical Engineering and Technology, Tianjin University, Tianjin 300072, China
[b] Collaborative Innovation Center of Chemical Science and Engineering (Tianjin), Tianjin 300072, China
[c] Tianjin Key Laboratory of Membrane Science and Desalination Technology, Tianjin University, Tianjin 300072, China

ARTICLE INFO

Keywords:
Polyhedral oligomeric silsesquioxanes (POSS)
Poly(ethylene glycol)
Nanocomposite membrane
Pervaporation
Ethanol dehydration

ABSTRACT

Fabrication of nanocomposite membranes with high nanoparticle loading is a significant challenge because of the serious agglomeration of nanoparticles at high concentration. In this study, poly(ethylene glycol)-functionalized polyoctahedral oligomeric silsesquioxanes (PEG@POSS) nanoparticles were incorporated into a sodium alginate (SA) matrix to fabricate nanocomposite membranes. A large loading of PEG@POSS up to 50 wt % with a well dispersion in the membrane was achieved due to the good compatibility between PEG@POSS and alginate chains. Benefiting from the nanostructured size of PEG@POSS (1–3 nm), the obtained nanocomposite membranes possessed very thin active layers of 180–200 nm. A large quantity of hydrophilic PEG side chains enhanced the membrane surface hydrophilicity and offered massive water binding sites in the membranes. Homogeneously dispersed high content PEG@POSS nanoparticles increased the free volume of the nanocomposite membranes while maintaining a suitable free volume cavity size for water permeation. The optimum separation performance with a permeation flux of 2500 g m^{-2} h^{-1} and a separation factor of 1077 for dehydration of 90/10 wt% ethanol/water feed was achieved. Additionally, the effects of operation temperature and feed concentration on separation performance were investigated systematically.

1. Introduction

Membrane separation technology has been widely used in the fields of water treatment, energy, food and chemical production for its energy-saving and environmental friendliness [1]. Organic-inorganic nanocomposite membranes, composed of organic polymers and inorganic fillers, have attracted much attention for their combination of both good film-forming and easy processing property of polymers and high selectivity benefited from inorganic particles [2]. A high performance nanocomposite membrane should at least have the following three structural features: (i) favorable compatibility between inorganic fillers and polymer matrix [2,3], (ii) well dispersion of inorganic fillers [4] and (iii) desirable/sufficient content of inorganic fillers [5,6]. To improve the compatibility between inorganic fillers and the polymer matrix, reducing the particle size is an efficient method. This is because nanoparticles provide larger interfacial areas per volume to contact the polymer chains [6–8]. However, nano-sized inorganic fillers tend to aggregate and generate non-selective interface voids, thus limiting the filling content and leading to a decrease of selectivity [9]. In order to improve the dispersion of fillers in membrane, several methods have been developed such as using a milder mixing process [5,10], in situ generation of nanoparticles within the polymer matrix [11,12] and in situ self-assembly driven by specific interactions [13]. However, these methods can only be applied to a narrow range of fillers. Surface modification of the fillers through pre-treatment such as polymer wrapping, silanizing and long-chain grafting is another effective strategy to achieve better filler dispersion in the membranes [9]. Modifying the filler surface with appropriate organic chains can enhance the compatibility between the fillers and polymer matrix as well as diminish the difference of thermal expansion coefficients of two phases which is further beneficial for homogenous dispersion of inorganic fillers [14]. However, due to the low grafting density, the traditional fillers after pre-modification usually still encounter serious agglomeration at higher loadings, making it difficult to control filler loading in a wide range. It is therefore of great significance to find suitable particle fillers with high grafting density for the fabrication of

* Corresponding author at: Key Laboratory for Green Chemical Technology of Ministry of Education, School of Chemical Engineering and Technology, Tianjin University, Tianjin 300072, China.
E-mail address: wuhong@tju.edu.cn (H. Wu).

http://dx.doi.org/10.1016/j.memsci.2017.05.040
Received 12 March 2017; Received in revised form 6 May 2017; Accepted 9 May 2017
Available online 18 May 2017

defect-free composite membranes with good filler dispersion at high loadings.

Polyhedral oligomeric silsesquioxanes (POSS) that contains an inner inorganic framework ($SiO_{1.5}$)x (x = 8, 10 or 12) cage and an external shell of organic substituent (R) embody an intrinsic inorganic–organic architecture [15]. POSS is considered as the smallest possible particles of silica with a nanostructured size of 1–3 nm in diameter [16]. The cage dimensions are ~0.54 nm along the body diagonal between Si atoms and ~0.32 nm along the edge between Si atoms [17]. Controllable organic substituents on the outer surface provide the possibility of good compatibility with diverse polymers at the molecular level by forming chemical/physical interactions [18–27]. The small size and intrinsic hybrid architecture of POSS highlight its potential advantages to achieve a high loading in the nanocomposite membranes without unfavorable aggregation and interface defects [25]. Prior to utilization of POSS materials, the rational choice of functionalized groups attached to the apex silicon atoms is a vital issue. For pervaporation dehydration application, hydrophilic particles are favored to prepare high-efficiency water-selective membranes because they possess abundant adsorption sites for water molecules [28–30]. Poly (ethylene glycol) (PEG) is distinctly hydrophilic and has been widely used in surface modification of nanofiltration and reverse osmosis membranes [31,32]. One water molecule can tightly bound with one ethylene glycol (EG) unit and form a strong hydration layer around PEG chains [33]. Therefore, it is reasonable to expect PEG-functioned POSS which can gather a large amount of water molecules around the PEG chains seems to be a creative alternative to harvest water molecules in the membranes. In addition, it is anticipated that high content of PEG@POSS could form a continuous hydrophilic water pathway in the membranes.

In this study, PEG(n)@POSS (n = 13.3) (as shown in Scheme 1) was blended with sodium alginate (SA) to fabricate nanocomposite membranes for pervaporative dehydration of ethanol. The morphology, interfacial interaction, crystallinity, free volume and hydrophilicity of the membranes were systematically characterized. Separation performance was evaluated using 90/10 wt% ethanol/water mixtures. The effects of PEG@POSS content, feed concentration and operating temperature on the membrane separation performance were thoroughly investigated.

2. Experimental

2.1. Materials

PEG@POSS was obtained from Yiyang Instrument and Management Department (Changsha, China). Sodium alginate was supplied by Qingdao Bright Moon seaweed Group Co. Ltd. (Shandong, China). Polyacrylonitrile (PAN) ultrafiltration membranes with a molecular weight cut-off of 100,000 were obtained from Shandong MegaVision Membrane Engineering & Technology Co. Ltd. (Shandong, China). Calcium chloride ($CaCl_2{\cdot}2H_2O$) and absolute ethanol (99.7 wt%) were purchased from Tianjin Guangfu Technology Development Co. Ltd. (Tianjin, China). All reagents were of analytical grade and used without further purification. Deionized water was used throughout the experiments.

Scheme 1. The chemical structure of PEG(n)@POSS (n = 13.3).

2.2. Membrane fabrication

The nanocomposite membranes were fabricated on PAN substrates via spin-coating method. PAN substrates were immersed in water for 24 h in advance to remove the residual glycerin. First, a certain amount of PEG@POSS was dispersed in 35 ml deionized water under stirring for 2 h at 303 K. Then, 0.525 g (mass ratio to water was 1.5 wt%) SA was added and stirred for another 4 h followed by filtration and degassing at room temperature. The above casting solution was spin-coated on PAN substrates and dried at room temperature for 24 h to evaporate the solvent. At last, the above-mentioned membranes were soaked in 0.5 M $CaCl_2{\cdot}2H_2O$ solution for 10 min with continuous stirring for cross-linking. The nanocomposite membranes were marked as SA-PEG@POSS(X)/PAN, where X represented the mass ratio of PEG@POSS to SA. Pristine SA membrane was also prepared for comparison. Homogeneous SA-PEG@POSS(X) membranes without PAN support were fabricated on glass plates for characterization.

2.3. Characterizations

The chemical structure of PEG@POSS was analyzed by Fourier transform infrared spectra with a scanning range of 4000–500 cm^{-1} and a resolution of 4 cm^{-1} (FT-IR, BRUKER Vertex 70). The morphology and cross-section image of the membrane were characterized by field emission microscopy (FESEM, Nanosem 430). Atomic force microscopy (AFM, CSPM5000) was used to detect the membrane surface morphology and surface roughness. Crystalline structure of membrane was figured out by Wide-angle X-ray diffraction patterns (XRD) through D/MAX-2500 X-ray diffractometer (CuKα) in the range of 2–70° with a scan rate of 5° min^{-1}. The phase transition behavior of the composite membranes was obtained by a Pyris Diamond differential scanning calorimetry (DSC, Netzsch 204 F1) under nitrogen flow with 10 K min^{-1} heating rate. The measurement of static contact angle of the membrane was performed at room temperature using a contact angle goniometer (JC2000C Contact Angle Meter).

Positron annihilation lifetime spectroscopy (PALS) measurement was used to investigate free volume cavity and fractional free volume. PALS measures the elapsed time between the implantation of the positron into the material and the emission of annihilation radiation. The positronium atom seeks out pores within the material where they are confined to bounce off the walls, and each time they collide with the walls, there is a probability of the atom being annihilated releasing γ-rays that can be detected. The lifetime of the positron is used to determine the pore size of the sample [34]. The whole system adopted EG & G ORTEC fast-slow coincidence system with a resolution of 209 ps. Two pieces of tested samples with an area of 1 × 1 cm^2 and a thickness of 0.5 mm were fixed on both sides of the radioactive source (13 μci ^{22}Na). Semiempirical equation derived by fitting the measured pick-off lifetime (τ) and free volume cavity in an infinite potential spherical model can be written in a general form as follows [34,35],

$$\tau_3 = \frac{1}{2}\left[1-\frac{r_3}{r_3+\Delta r}+\left(\frac{1}{2\pi}\right)sin\left(\frac{2\pi r_3}{r_3+\Delta r}\right)\right]^{-1} \quad (1)$$

$$f_{app} = \frac{4\pi}{3}r_3^3 I_3 \quad (2)$$

where r_3 is the mean free-volume radius (nm), Δr is the electron layer thickness for the positron (calibrated to be 0.1656 nm), f_{app} and I_3 are the fractional free volume of membrane and intensity of o-Ps (%), respectively.

2.4. Swelling and pervaporation experiment

Homogeneous membranes were dried in vacuum oven at 313 K for 72 h until their mass remained constant. The membranes were then immersed in 90 wt% ethanol aqueous solution at 350 K for 48 h to achieve equilibrium. The swollen membranes were weighed. The swelling degree (SD, %) was calculated by the following formula,

$$SD = \frac{M_S - M_D}{M_D} \times 100 \quad (3)$$

where M_D and M_S were the weights of dry and swollen membranes (g), respectively.

Pervaporation experiments were conducted on the equipment described previously [36]. The key part in the membranous cisterns was P-28 membrane module (CM-Celfa AG Company, Switzerland) with an effective membrane area (A) of 25.6 cm^2. The feed circulated through the membrane surface at a flow rate of 60 L/h while the pressure on the permeate side was kept at 0.3 KPa by a vacuum pump. A liquid nitrogen cold trap was used to collect the permeate vapor every 30 min. All the experiments were repeated three times to obtain an average data. The compositions of feed and permeate solutions were determined by gas chromatography (Agilent7890, USA). Separation performance was evaluated in terms of permeation flux (J, g m^{-2} h^{-1}) and separation factor (α) as follows,

$$J = \frac{Q}{A \times t} \quad (4)$$

$$\alpha = \frac{P_W/P_E}{F_W/F_E} \quad (5)$$

where Q was the average mass of permeate (g). P and F represented the mass fractions of water (subscript W) and ethanol (subscript E) on the permeation and feed side, respectively.

In order to clarify the separation property of the membrane material itself, permeance of individual components $(P/l)_i$ (GPU, 1GPU = 7.501×10^{-12} m^3(STP)/m^2 s Pa) and selectivity (β) were further calculated by following equations [37],

$$(P/l)_i = \frac{J_i}{p_{io} - p_{il}} = \frac{J_i}{\gamma_{io}\chi_{io}p_{io}^{sat} - p_{il}} \quad (6)$$

$$\beta = \frac{(P/l)_w}{(P/l)_E} \quad (7)$$

where J_i was the permeation flux of component i (g m^{-2} h^{-1}), l was membrane thickness (m), p_{io} and p_{il} were the partial pressures on the feed side and permeate side of component i (Pa), respectively. γ_{io} and χ_{io} were the activity coefficient and molar ratio of component i on the feed side (calculated via Aspen simulation), p_{io}^{sat} was the saturated vapor pressure of pure component i (Pa). The permeation flux of water and ethanol was transformed into volumes under standard temperature and pressure (STP), 1.245 m^3 (STP) for 1 kg water vapor and 0.487 m^3 (STP) for 1 kg ethanol vapor.

3. Results and discussion

3.1. Surface morphology of the membranes

The membrane surface morphology was characterized by FESEM as shown in Fig. 1. SEM image of the PAN support was shown in Fig. 1(e). Numerous nanopores (15 nm in average) with homogenous distribution existed on the surface of the PAN ultrafiltration membrane. After the deposition process, all the pores were covered and a defect-free layer was formed as shown in Fig. 1(a)-(d). Due to the small size and good compatibility between PEG@POSS and SA, all the nanocomposite membranes showed smooth and dense surface similar to the pristine SA membrane. No bulky agglomeration and interface defects were observed on the surface even at high loadings. The digital pictures of the corresponding homogeneous membranes were also shown on the right corner of the figure. Compared with the transparent pristine SA membrane, the SA-PEG@POSS nanocomposite membranes were opaque white and the transparency decreased gradually with an increase of PEG@POSS loading. The existence of Si element in SEM-EDX (Fig. 1(g)-(h)) confirmed the involvement of PEG@POSS in the nanocomposite membranes. In addition, the C and O elements from the SA matrix and PEG side segment were also detected. The Ca element was from the $CaCl_2$ used in cross-linking. Fig. 2 showed the cross-section images of the composite membranes and PAN substrate. The thin active layers were dense, uniform and tightly adhered to the porous PAN substrates. The thicknesses of the active layer were only 180–200 nm which were less than most of the nanocomposite membranes prepared by spin coating method [38–40]. The thin active layers are beneficial for molecule permeation by reducing the transport resistance to get a high permeation flux.

AFM was used to obtain further understanding of the surface morphology. The calculated surface roughness parameters were listed in Table 1. R_a, R_q and R_z represented the average deviation of height, the root mean square deviation of height and the maximum vertical distance between the highest and the lowest point on membrane surface respectively. The surface roughness of the nanocomposite membrane was higher than that of the pristine SA membrane. This increase was probably due to the interaction between the PEG segments and the SA chains which led to the reorganization of SA chains in the presence of PEG@POSS [25]. When the filler loading exceeded 30 wt%, a large amount of soft PEG chains would locate on the membrane surface, resulting in the downward trend of surface roughness at high loading.

3.2. Chemical structure of the membranes

The FT-IR spectra of PEG@POSS and nanocomposite membranes were depicted in the Fig. 3. The strong adsorption bands at 2850 cm^{-1} and 1460 cm^{-1} were originated from the stretching vibrations of C–H bond and vibration absorption of -CH_2-CH_2- on the PEG chains respectively. The strong band at 1105 cm^{-1} was assigned to stretching vibrations of -Si-O-Si- groups in the silsesquioxane cages [41]. For the pristine SA membrane, three characteristic bands at 3350 cm^{-1}, 1610 cm^{-1} and 1400 cm^{-1} were ascribed to the stretching vibration of hydroxyl group, symmetric and asymmetric stretching vibration of carboxylate salt respectively [38]. These characteristic bands of SA were observed on the spectra of nanocomposite membranes and no bands for PEG@POSS were observed owing to its quite small size.

Raman spectra of PEG@POSS and nanocomposite membranes in the range of 500 cm^{-1}-2500 cm^{-1} were recorded and are shown in Fig. 4. For the normal pristine SA membrane, three characteristic peaks observed at 1098 cm^{-1}, 1300 cm^{-1} and 1413 cm^{-1} were attributed to the vibrations of the polymer backbone, C–O single bond stretching and symmetric vibration of carboxylate group respectively [42]. The bands at 1040 cm^{-1} and 1464 cm^{-1} appeared in the spectra of nanocomposite membranes were assigned to the -Si-O-Si- stretching mode in the silsesquioxane cages and -CH_2-O- groups in the PEG side chains, revealing the presence of PEG@POSS in the SA matrix [43].

3.3. Physical structure of the membranes

XRD was used to evaluate the crystalline property of the membranes as shown in Fig. 5. All the nanocomposite membranes and pristine SA membranes showed two broad characteristic peaks at $2\theta = 23^\circ$ and $2\theta = 17^\circ$ revealing the semi-crystalline region of the polymer matrix. [35]. No typical diffraction peaks of PEG@POSS appeared, probably

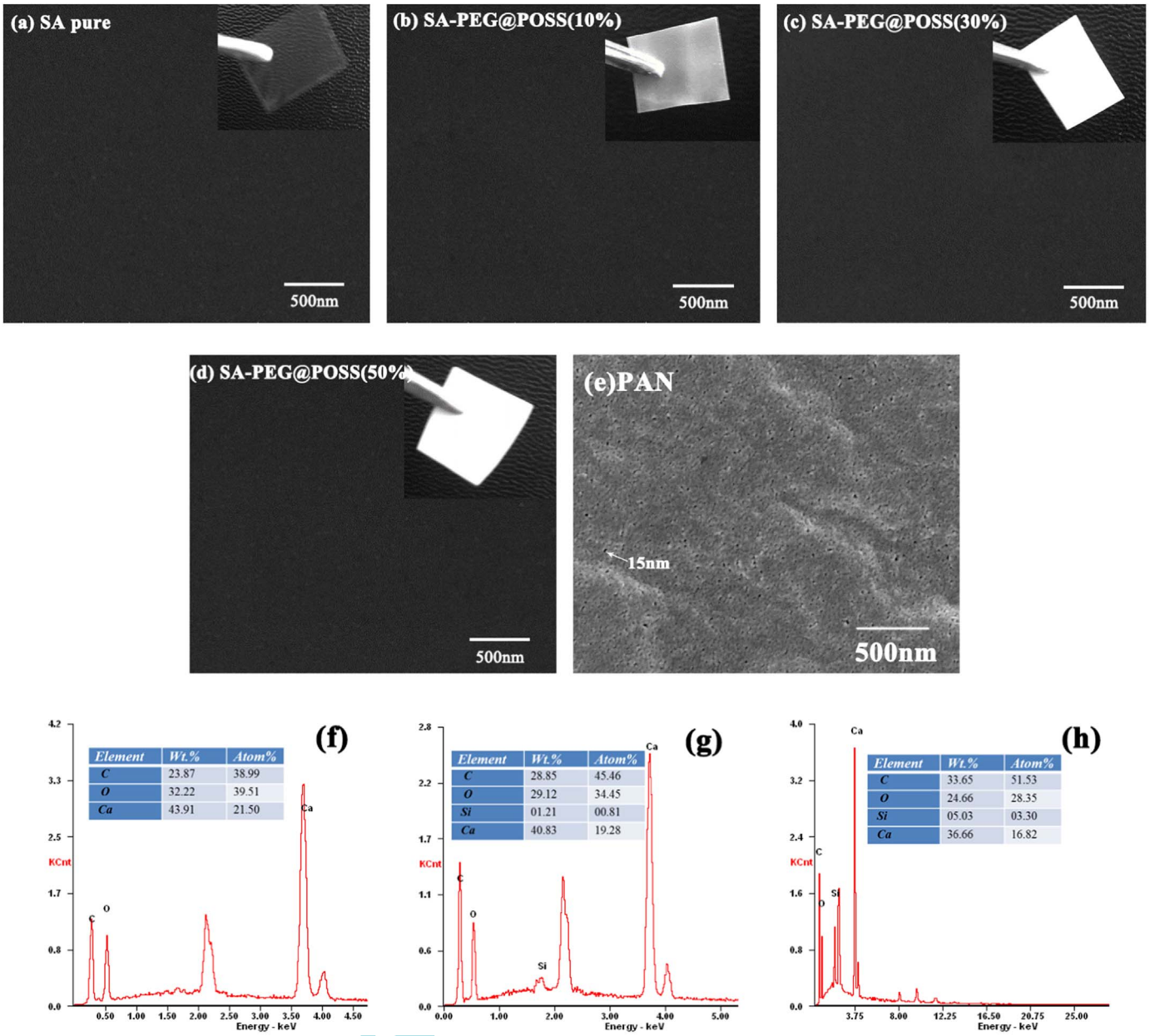

Fig. 1. SEM images of surface morphology of (a) SA; (b) SA-PEG@POSS(10%); (c) SA-PEG@POSS(30%) and (d) SA-PEG@POSS(50%) (e) PAN substrate; EDX images of (f) SA; (g) SA-PEG@POSS(10%); (h) SA-PEG@POSS(30%).

because the characteristic broad diffraction peak of PEG(n)@POSS (n = 13.3) at 2θ = 22° overlapped the characteristic peak of sodium alginate, which made it difficult to be observed in the membranes [44] PEG@POSS existed in an amorphous form and dispersed homogeneously in the composite membranes. With the increase of PEG@POSS content, the intensity of crystalline peak decreased gradually. The existence of POSS cages and hydrogen bonds formed between SA chains and PEG chains (-OH groups of SA and -O- groups of PEG chains) disrupted the original ordered packing of stiff SA chains, leading to a decrease of crystalline region and an increase of amorphous region in SA matrix [39,45].

Glass transition temperature (T_g) was estimated by DSC measurement to explore the chain mobility and rigidity. As displayed in Fig. 6. The T_g value decreased first when the filler loading was below 30% and then increased with the augment of PEG@POSS content. The decrease of T_g could be explained as follows: (1) the addition of PEG@POSS disturbed the inherent organization of SA chains [20,45]; (2) the introduced soft PEG side chains had higher chain mobility than alginate chains [46]. However, with further increasing of PEG@POSS content, hydrogen bond interaction between SA chains and PEG side chains constrained the movement of SA chains and overwhelmed the above two effects, thus leading to the increase of chain stiffness and T_g at higher loading content.

Free volume characteristics measured by PALS have been proven to be efficient and powerful to analyze molecular separation performance of composite membranes. The free volume parameters were listed in Table 2. The parameters r_3 and I_3 were the radius and intensity of small cavities (also called network cavities) between the polymer chains, respectively. The cavity size r_3 increased progressively at first and then declined after the filler content was higher than 30%, while the intensity I_3 decreased a little bit and then increased all along. The fractional free volume (f_{app}) reached its maximum at 30% PEG@POSS loading, which was 37% higher than that for pristine SA membrane. The incorporation of PEG@POSS disturbed the chains packing and made larger hole in the amorphous region of the membranes, thereby leading to larger free volume cavities between alginate chains. Mean-

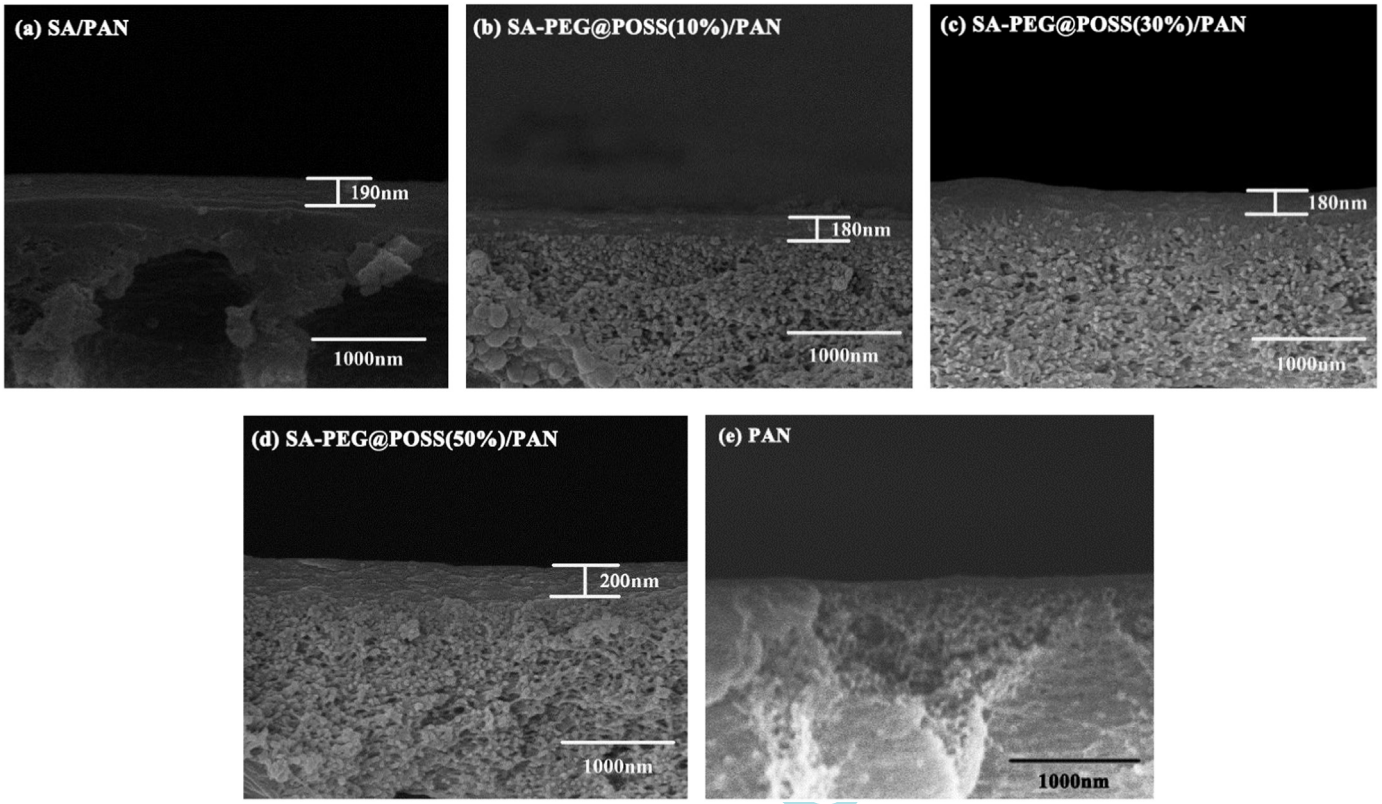

Fig. 2. SEM images of cross-section morphology of (a) SA/PAN; (b) SA-PEG@POSS(10%)/PAN; (c) SA-PEG@POSS (30%)/PAN and (d) SA-PEG@POSS (50%)/PAN (e) PAN substrate.

Table 1
The surface roughness of SA/PAN and SA-PEG@POSS(X)/PAN membranes.

Membrane	Roughness		
	Ra (nm)	*Rq* (nm)	*Rz* (nm)
SA	11.57	14.33	119.41
SA-PEG@POSS (10%)	14.08	18.44	124.98
SA-PEG@POSS (30%)	15.23	19.21	177.69
SA-PEG@POSS (50%)	13.52	16.87	176.23

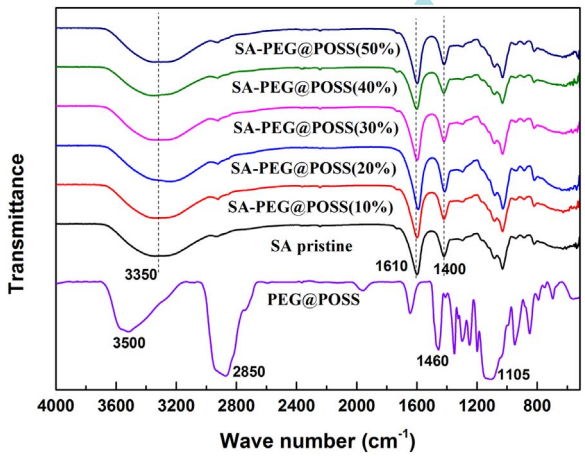

Fig. 3. FT-IR spectra of PEG@POSS and nanocomposite membranes.

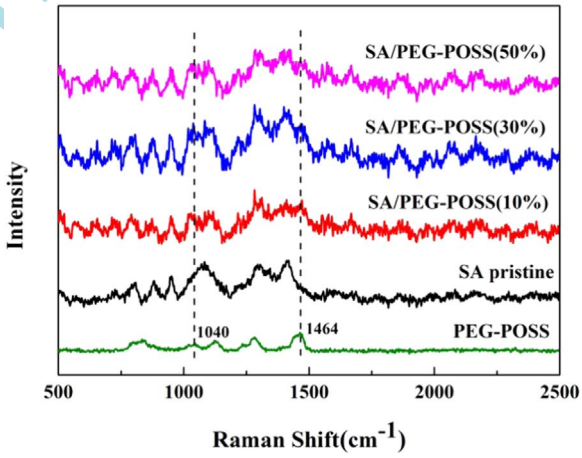

Fig. 4. Raman spectra of PEG@POSS and nanocomposite membranes.

while, the hydrogen bond between PEG and SA restricted the chain mobility, conferring the membrane with a more compact structure and smaller free volume cavities [28]. The restriction effect of hydrogen bonds was obvious and responsible for the decrease of free volume at higher loadings. Moreover, the cage-like structure of POSS made by single -Si–O–Si- unit might increase the fractional free volume to some extent [47]. It's worth noting that the free volume cavity radius of the nanocomposite membranes was in the range of 0.261–0.287 nm, much larger than the kinetic radius of water molecule (0.13 nm), benefiting water to permeate easier than ethanol molecule (0.23 nm) through the membranes [35].

3.4. Hydrophilicity and swelling property of the membranes

Water static contact angles were used to characterize the hydrophilicity of the membranes and results were shown in Fig. 7. The contact angle of pristine SA membrane was 36°. After incorporation of PEG@POSS, the contact angle remarkably decreased to 22° at the filler loading of 20%. The increase of surface hydrophilicity of nanocomposite membranes was due to the hydrophilic PEG chains spreading on the surface of the membranes. When the PEG@POSS loading was higher

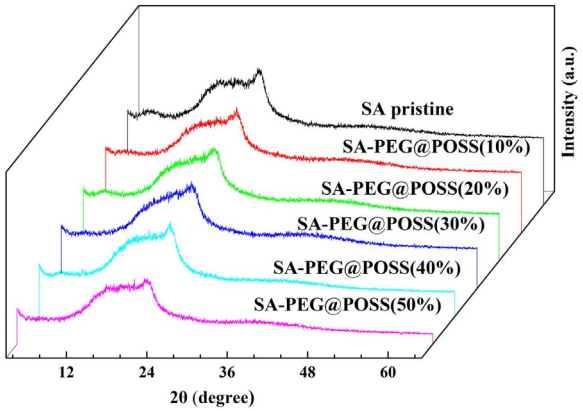

Fig. 5. Wide-angle X-ray diffraction curves of SA pristine and SA-PEG@POSS(X) membranes.

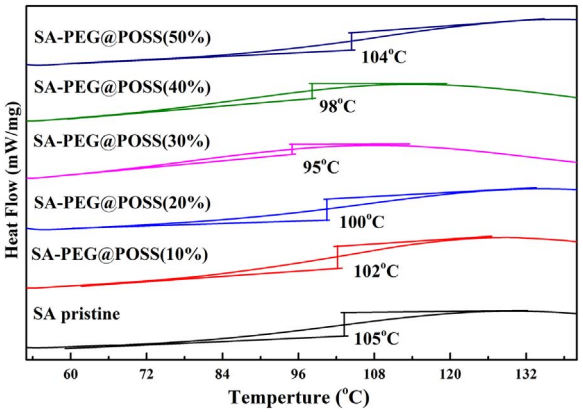

Fig. 6. DSC curves of SA pristine and SA-PEG@POSS(X) membranes.

Table 2
Free volume property of SA pristine and SA-PEG@POSS(X) membranes.

membrane	I_3 (%)	τ (ns)	r_3 (nm)	f_{app} (%)
SA	8.07	1.709	0.257	0.571
SA-PEG@POSS (10%)	7.46	1.827	0.269	0.605
SA-PEG@POSS (30%)	7.88	2.025	0.287	0.781
SA-PEG@POSS (50%)	8.10	1.751	0.261	0.602

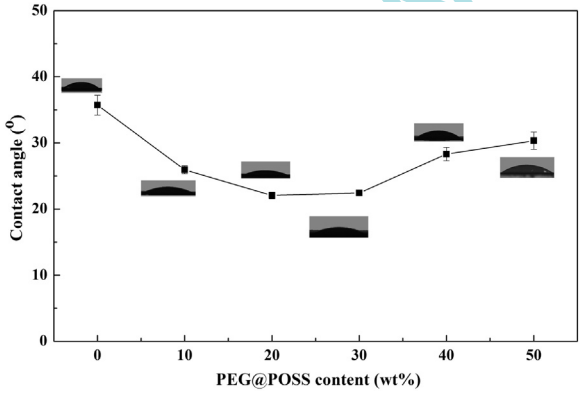

Fig. 7. Water contact angle of SA/PAN and SA-PEG@POSS(X)/PAN membranes.

than 30%, interfacial interaction between large amount of PEG chains and SA chains reduced the amount of effective hydrophilic groups exposed on the surface, thus the water contact angle increased slightly [21]. Nevertheless, all composite membranes exhibited better hydrophilicity than that of the pristine SA membrane, suggesting better affinity with water and enhanced separation factor.

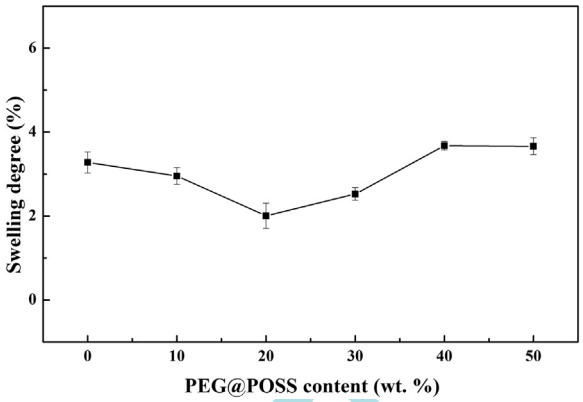

Fig. 8. Swelling degree of SA pristine and SA-PEG@POSS(X) membranes.

Swelling behavior is key factor affecting the long-term operation stability of membranes. As illustrated in Fig. 8, both the pristine SA membrane and the nanocomposite membranes displayed quite low swelling degrees (< 4%) with a small fluctuation which was favorable for practical application.

3.5. Pervaporation performance of the membranes

3.5.1. Effect of PEG@POSS content

Water/ethanol mixture (90/10 wt%) was used as the feed to investigate the separation performance of membranes at 350 K (Fig. 9). The permeation flux and separation factor for pristine SA membrane was 1810 g m^{-2} h^{-1} and 653, respectively. Both the permeation flux and separation factor increased synchronously after incorporating PEG@POSS, and reached maximum at 30% loading with a permeation flux of 2500 g m^{-2} h^{-1} and a separation factor of 1077, and then decreased at higher loadings.

The structure of the nanocomposite membranes was schematically illustrated in Scheme 2. One ethylene glycol (EG) unit could bind one water molecule through hydrogen bond and form a hydration layer along the PEG chain. Herein, PEG(n = 13.3) was used to modify POSS (PEG(n)@POSS (n = 13.3)), i.e., at most 104 water molecules could gather around the PEG chains. This PEG modification helped greatly to harvest water molecules in the membrane, especially at high loading of PEG@POSS up to 30%. In addition, the decreased crystallinity and increased fractional free volume provided the water molecules with fast transport pathways in the free volume cavities between the polymer chains, leading to the enhancement of permeation flux. The enhanced surface hydrophilicity of the nanocomposite membranes after incorporation of PEG@POSS would preferentially adsorb water molecules

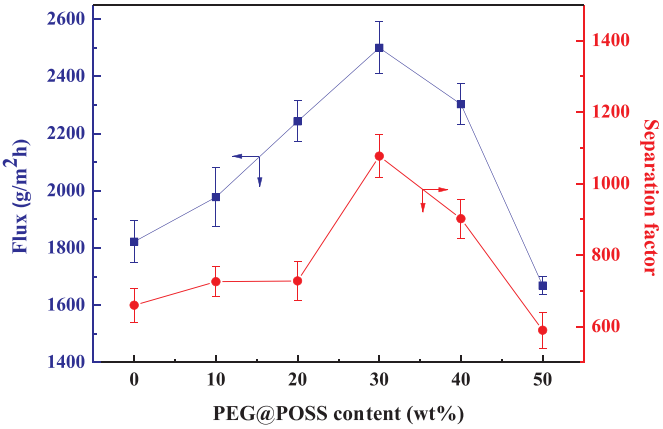

Fig. 9. Effect of PEG@POSS content on pervaporation performance of membranes.

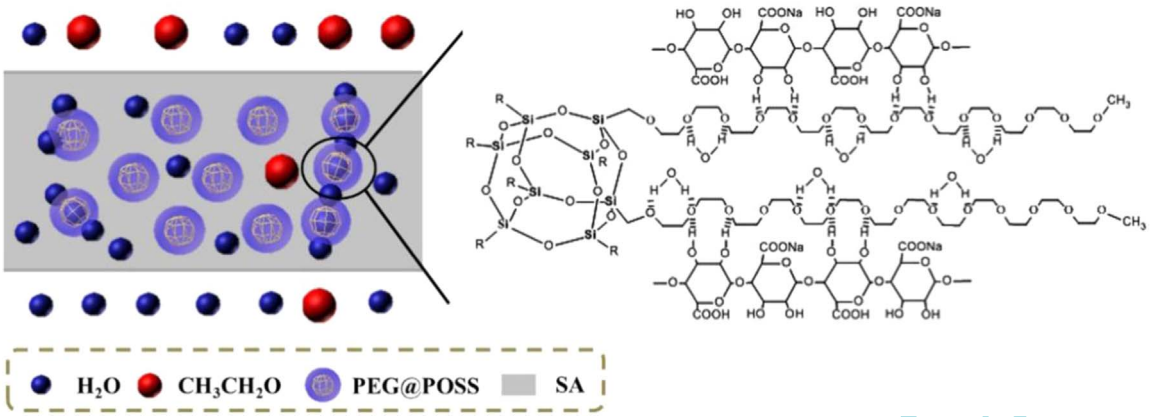

Scheme 2. Schematic diagram of water permeation in nanocomposite membrane.

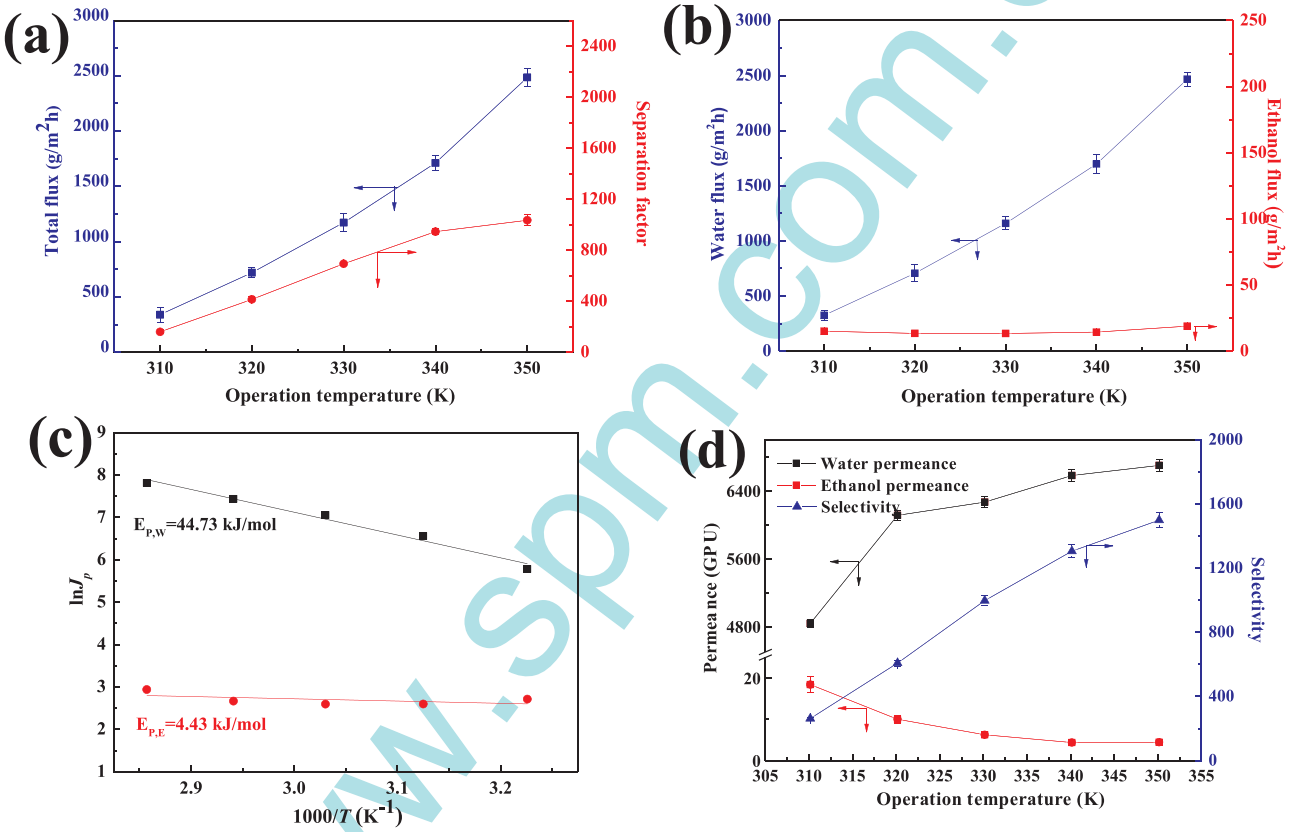

Fig. 10. Effect of feed temperature on separation performance of SA-PEG@POSS(30%)/PAN membrane: (a) total flux and separation factor; (b) water flux and ethanol flux; (c) Arrhenius plots of water and ethanol; and (d) water permeance, ethanol permeance and selectivity.

and repel ethanol molecules in the meantime, and thus the adsorption selectivity was also enhanced. Furthermore, the ethanol molecules would encounter more transfer resistance than that of water molecules in the composite membrane because free volume cavity radius of the nanocomposite membranes was in the range of 0.261–0.287 nm, only slightly larger than the kinetic radius of ethanol molecule (0.23 nm) and much larger than the kinetic radius of water molecule (0.13 nm). With further addition of PEG@POSS, the relative content of SA decreased, hydrophilic groups would be replaced by the hydrogen bond between PEG chains and alginate chains, endowing the membrane with less adsorption selectivity. Massive POSS cages embedded in the polymer network would make the diffusion pathways more tortuous for both water molecules and ethanol molecules [27]. Consequently, the permeation flux and separation factor declined simultaneously at high loading contents.

3.5.2. *Effect of operation temperature*

The effect of operation temperature on the separation performance of the SA-PEG@POSS(30%)/PAN membrane was investigated in the range of 310–350 K for 90 wt% water/ethanol feed. As shown in Fig. 10(a) and (b), the total permeation flux, water permeation flux and separation factor increased continuously with the increase of temperature while the ethanol permeation flux remained constant. The temperature exerts its influence on separation performance from the following three aspects. (1) Elevated temperature would promote the molecular thermal movement and chain mobility of alginate, thus enhancing the permeation flux. (2) The saturated vapor pressure increased with the increase of temperature at the feed side while the permeate side kept vacuum constant, so the driving force for mass transport was enhanced. (3) High temperature would suppress the solubility of molecules. For water permeation, the positive effect of

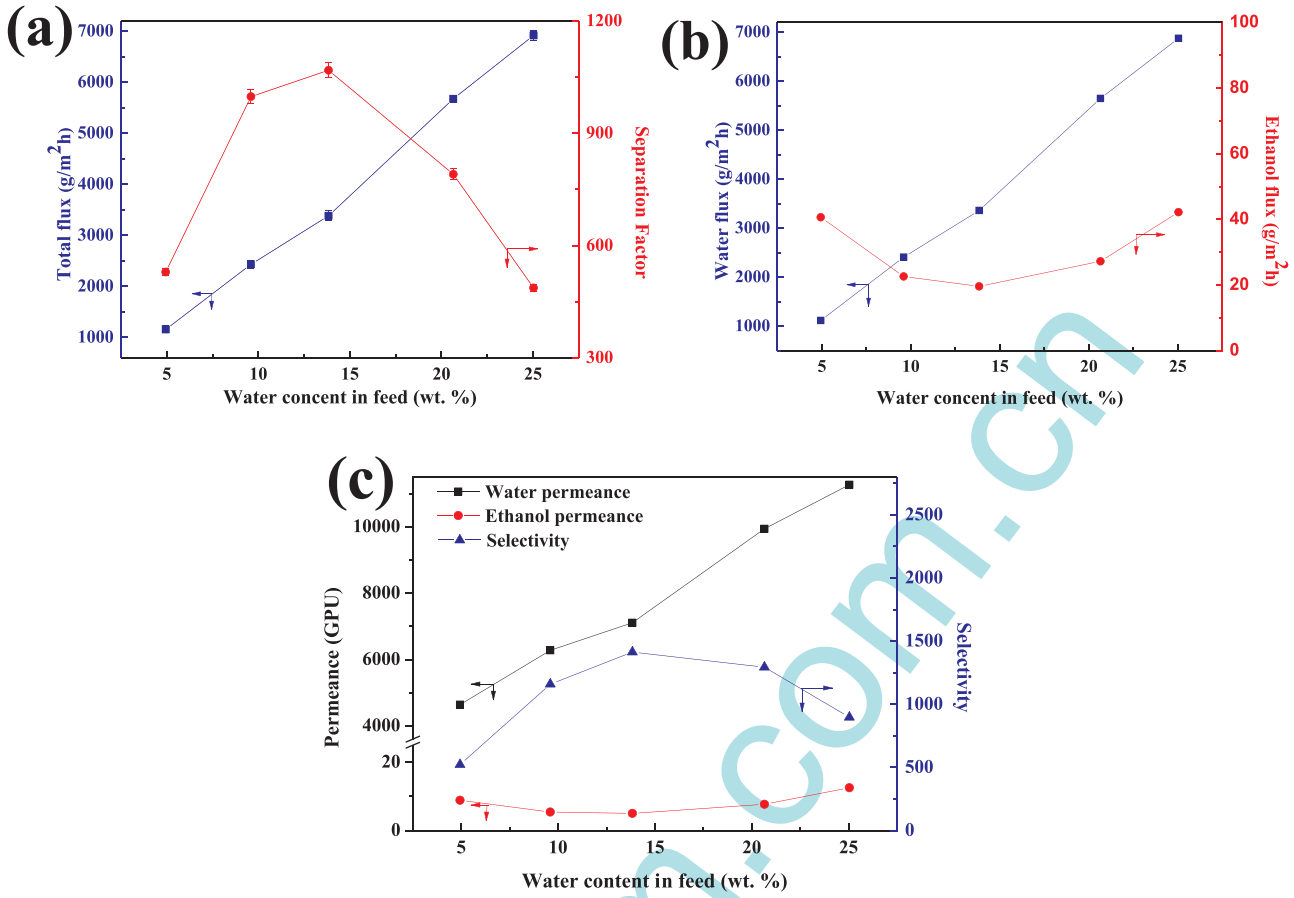

Fig. 11. Effect of feed composition on separation performance of SA-PEG@POSS (30%)/PAN membrane: (a) total flux and separation factor; (b) water flux and ethanol flux; (c) water permeance, ethanol permeance and selectivity.

Table 3
Comparison of separation performance of silica materials-incorporated nanoconposite membranes for ethanol dehydration.

Nanoparticles	Polymer	Water content (wt%)	Feed temperature (K)	Permeation flux (g m^{-2} h^{-1})	Separation factor	Reference
Aminopropylphenyl POSS	6FDA-NDA/DABA	15	333	1900	166	[45]
Silica nanoparticles	PEI/SA	10	349	1490	2050	[11]
Disilanolisobutyl POSS	6FDA-NDA/DABA	15	333	2000	137	[27]
Phenyltriethoxysilane	PVA	15	313	145	1026	[12]
Diethoxydiphenylsilane	PVA	15	313	141	248	
Silica MCM-41	PI Matrimid®5218	10	315	440	252	[48]
Mesoporous silica-(ZIF-8)	PI Matrimid®5218	10	315	200	137	
Mesoporous silica	PVA	10	333	855	42	[49]
PEG@POSS	SA	10	350	2500	1077	This work

both (1) and (2) triumphed over the negative effect of (3), while for ethanol, the increasing effect of both (1) and (2) balanced the decreasing effect of (3). Consequently, water permeation flux increased remarkably while ethanol permeation flux retained almost unchanged.

Arrhenius equation was employed to further describe the effect of temperature on permeation flux, and the apparent activation energy was figured out by the slope of the fitted curves [38],

$$J_P = A_P \exp\left(-\frac{E_P}{RT}\right) \quad (8)$$

where A_P, J_P, E_P, R and T were the pre-exponential factor, permeation flux, apparent activation energy, gas constant and feed temperature, respectively. The fitted curves of $\ln J_P$ versus 1000/T were shown in Fig. 10(c). The apparent activation energy for water and ethanol were 44.73 kJ/mol and 4.43 kJ/mol, respectively. The higher apparent activation energy for water implied that water flux would increase more rapidly than the ethanol flux with increasing temperature. Fig. 10(d) revealed the effect of temperature on the permeance and selectivity with normalized driving force. With the increasing temperature, water permeance showed a sustained increase while ethanol permeance declined a little bit, which further proved that the accelerated diffusion process in the membrane played a dominant role for water permeation, while the suppressed adsorption process on the membrane surface had a more crucial effect on the ethanol permeation.

3.5.3. Effect of feed composition

The effect of feed composition with a water concentration of 5–25% on the separation performance of the SA-PEG@POSS(30%)/PAN membrane was investigated at 350 K. As shown in Fig. 11(a) and (b), the total flux and water flux increased monotonously while ethanol flux declined at first and then rose with the increase of water content. The driving force for water transport increased with the increased water concentration in the feed. Therefore, the water permeation flux increased while the ethanol permeation flux decreased. However, at

higher water content, the significant plasticization effect on polymer matrix facilitated the transport of both water molecules and ethanol molecules [39]. As a result, the ethanol flux showed an increasing tendency. To further investigate the effect of feed content on the separation performance, membrane flux and separation factor were normalized to permeance and selectivity, respectively. As shown in Fig. 11(c), the ethanol permeance remained constant at low water content and then increased, while the water permeance kept increasing, confirming the plasticization effect of water on membrane structure. When water concentration was less than 15%, the low swelling of membrane exerted little effect on ethanol permeation. At higher water contents, the inter-chain space became larger to facilitate ethanol transfer. Consequently, selectivity increased at first but then declined with increasing water concentration in feed. A desirable pervaporation performance was achieved at 25% water content, the total flux reached 6919 g m^{-2} h^{-1} while the water content on the permeate side maintained higher than 99 wt%.

3.6. Comparison with literature data

A comparison of the separation performance of silica materials-incorporated nanoconposite membranes for ethanol dehydration was made as listed in Table 3. The PEG@POSS-doped alginate nanocomposite membrane prepared in this study showed outstandingly high separation performance for ethanol dehydration.

4. Conclusion

In this study, PEG-modified POSS was introduced into alginate matrix to fabricate nanocomposite membranes for ethanol dehydration. The nano size of POSS cage and good compatibility between PEG chains and alginate chains allowed a high doping content up to 50% in the nanocomposite membranes. SEM images indicated that a thin nanocomposite layer with the thickness of 200 nm deposited onto PAN porous support layer. The PEG chains on POSS cages enhanced the membrane hydrophilicity and offered a large amount of water binding sites in the membranes. In addition, the incorporation of PEG@POSS decreased the crystallinity of adjacent alginate chains and improved the free volume property of membranes. The nanocomposite membrane with PEG@POSS content of 30% showed the optimal permeation flux of 2500 g m^{-2} h^{-1} and a separation factor of 1077, which were 1.3 and 1.5 times higher than pristine SA membrane. This study reveals that properly functionalized POSS materials may find promising potential in the development of highly loaded ultrathin high-performance nanocomposite membranes for gas and liquid separation.

Acknowledgements

The author appreciates the financial support from the National Natural Science Foundation of China (21576189, 21490583, 213906131 and 21621004), Natural Science Foundation of Tianjin (16JCZDJC36500), National Science Fund for Distinguished Young Scholars (21125627), State Key Laboratory of Separation Membranes and Membrane Processes (Tianjin Polytechnic University) (M2-201504, M2-201606), Tianjin Application Foundation and Research in Cutting-edge Technology Plan (15JCQNJC43300), the Programme of Introducing Talents of Discipline to Universities (No. B06006).

References

[1] Y.K. Ong, G.M. Shi, N.L. Le, Y.P. Tang, J. Zuo, S.P. Nunes, T.S. Chung, Recent membrane development for pervaporation processes, Prog. Polym. Sci. 57 (2016) 1–31.
[2] V.T. Hoang, S. Kaliaguine, Predictive models for mixed-matrix membrane performance: a review, Chem. Rev. 113 (2013) 4980–5028.
[3] M. Rezakazemi, A. Ebadi Amooghin, M.M. Montazer-Rahmati, A.F. Ismail, T. Matsuura, State-of-the-art membrane based CO_2 separation using mixed matrix membranes (MMMs): an overview on current status and future directions, Prog. Polym. Sci. 39 (2014) 817–861.
[4] P.S. Goh, A.F. Ismail, S.M. Sanip, B.C. Ng, M. Aziz, Recent advances of inorganic fillers in mixed matrix membrane for gas separation, Sep. Purif. Technol. 81 (2011) 243–264.
[5] Y.H. Deng, J.T. Chen, C.H. Chang, K.S. Liao, K.L. Tung, W.E. Price, Y. Yamauchi, K.C.W. Wu, A. Drying-Free, Water-based process for fabricating mixed-matrix membranes with outstanding pervaporation performance, Angew. Chem. Int. Ed. 55 (2016) 12793–12796.
[6] R.D. Noble, Perspectives on mixed matrix membranes, J. Membr. Sci. 378 (2011) 393–397.
[7] T.S. Chung, L.Y. Jiang, Y. Li, S. Kulprathipanja, Mixed matrix membranes (MMMs) comprising organic polymers with dispersed inorganic fillers for gas separation, Prog. Polym. Sci. 32 (2007) 483–507.
[8] R. Nasir, H. Mukhtar, Z. Man, D.F. Mohshim, Material advancements in fabrication of mixed-matrix membranes, Chem. Eng. Technol. 36 (2013) 717–727.
[9] Y. Li, G. He, S. Wang, S. Yu, F. Pan, H. Wu, Z. Jiang, Recent advances in the fabrication of advanced composite membranes, J. Mater. Chem. A 1 (2013) 10058–10077.
[10] H.W. Fan, Q. Shi, H. Yan, S.L. Ji, J.X. Dong, G.J. Zhang, Simultaneous spray self-assembly of highly loaded ZIF-8-PDMS nanohybrid membranes exhibiting exceptionally high biobutanol-permselective pervaporation, Angew. Chem. Int. Ed. 53 (2014) 5578–5582.
[11] G.H. Liu, Z.Y. Jiang, X.X. Cheng, C. Chen, H. Yang, H. Wu, F.S. Pan, P. Zhang, X.Z. Cao, Elevating the selectivity of layer-by-layer membranes by in situ bioinspired mineralization, J. Membr. Sci. 520 (2016) 364–373.
[12] L.L. Xia, C.L. Li, Y. Wang, In-situ crosslinked PVA/organosilica hybrid membranes for pervaporation separations, J. Membr. Sci. 498 (2016) 263–275.
[13] R. Zhang, S. Ji, N. Wang, L. Wang, G. Zhang, J.R. Li, Coordination-driven in situ self-assembly strategy for the preparation of metal-organic framework hybrid membranes, Angew. Chem. 53 (2014) 9775–9779.
[14] V.C. Souza, M.G.N. Quadri, Organic-inorganic hybrid membranes in separation processes: a 10-year review, Braz. J. Chem. Eng. 30 (2013) 683–700.
[15] G.Z. Li, L.C. Wang, H.L. Ni, C.U. Pittman, Polyhedral oligomeric silsesquioxane (POSS) polymers and copolymers: a review, J. Inorg. Organomet. Polym. 11 (2001) 123–154.
[16] D.B. Cordes, P.D. Lickiss, F. Rataboul, Recent Developments in the Chemistry of Cubic Polyhedral Oligosilsesquioxanes, Chem. Rev. 110 (2010) 2081–2173.
[17] M.H. Lamm, T. Chen, S.C. Glotzer, Simulated assembly of nanostructured organic/inorganic networks, Nano Lett. 3 (2003) 989–994.
[18] Y. Li, T.S. Chung, Molecular-level mixed matrix membranes comprising Pebax (R) and POSS for hydrogen purification via preferential CO_2 removal, Int. J. Hydrog. Energy 35 (2010) 10560–10568.
[19] D. Xu, L.S. Loo, K.A. Wang, Pervaporation performance of novel chitosan-POSS hybrid membranes: effects of POSS and operating conditions, J. Polym. Sci. Part B: Polym. Phys. 48 (2010) 2185–2192.
[20] N.L. Le, Y. Wang, T.S. Chung, Pebax/POSS mixed matrix membranes for ethanol recovery from aqueous solutions via pervaporation, J. Membr. Sci. 379 (2011) 174–183.
[21] D. Xu, L.S. Loo, K. Wang, Characterization and diffusion behavior of chitosan-POSS composite membranes, J. Appl. Polym. Sci. 122 (2011) 427–435.
[22] Q.G. Zhang, B.C. Fan, Q.L. Liu, A.M. Zhu, F.F. Shi, A novel poly(dimethyl siloxane)/poly(oligosilsesquioxanes) composite membrane for pervaporation desulfurization, J. Membr. Sci. 366 (2011) 335–341.
[23] M. Dalwani, J.M. Zheng, M. Hempenius, M.J.T. Raaijmakers, C.M. Doherty, A.J. Hill, M. Wessling, N.E. Benes, Ultra-thin hybrid polyhedral silsesquioxane-polyamide films with potentially unlimited 2D dimensions, J. Mater. Chem. 22 (2012) 14835–14838.
[24] D. Gupta, A. Madhukar, V. Choudhary, Effect of functionality of polyhedral oligomeric silsesquioxane POSS on the properties of sulfonated poly(ether ether ketone) SPEEK based hybrid nanocomposite proton exchange membranes for fuel cell applications, Int. J. Hydrog. Energy 38 (2013) 12817–12829.
[25] M.M. Rahman, V. Filiz, S. Shishatskiy, C. Abetz, S. Neumann, S. Bolmer, M.M. Khan, V. Abetz, PEBAX (R) with PEG functionalized POSS as nanocomposite membranes for CO_2 separation, J. Membr. Sci. 437 (2013) 286–297.
[26] R. Konietzny, T. Koschine, K. Ratzke, C. Staudt, POSS-hybrid membranes for the removal of sulfur aromatics by pervaporation, Sep. Purif. Technol. 123 (2014) 175–182.
[27] N.L. Le, T.S. Chung, High-performance sulfonated polyimide/polyimide/ polyhedral oligosilsesquioxane hybrid membranes for ethanol dehydration applications, J. Membr. Sci. 454 (2014) 62–73.
[28] J. Zhao, Y.W. Zhu, G.W. He, R.S. Xing, F.S. Pan, Z.Y. Jiang, P. Zhang, X.Z. Cao, B.Y. Wang, Incorporating zwitterionic graphene oxides into sodium alginate membrane for efficient water/alcohol separation, ACS Appl. Mater. Interfaces 8 (2016) 2097–2103.
[29] L. Shan, L. Gong, H. Fan, S. Ji, G. Zhang, Spray-assisted biomineralization of a superhydrophilic water uptake layer for enhanced pervaporation dehydration, J. Membr. Sci. 522 (2017) 183–191.
[30] G.R. Wu, M.C. Jiang, T.T. Zhang, Z.Q. Jia, Tunable pervaporation performance of modified MIL-53(Al)-NH2/Poly(vinyl alcohol) mixed matrix membranes, J. Membr. Sci. 507 (2016) 72–80.
[31] B.D. McCloskey, H.B. Park, H. Ju, B.W. Rowe, D.J. Miller, B.D. Freeman, A bioinspired fouling-resistant surface modification for water purification membranes, J. Membr. Sci. 413 (2012) 82–90.
[32] G.D. Kang, H.J. Yu, Z.N. Liu, Y.M. Cao, Surface modification of a commercial thin film composite polyamide reverse osmosis membrane by carbodiimide-induced

grafting with poly(ethylene glycol) derivatives, Desalination 275 (2011) 252–259.
[33] J. Wu, S.F. Chen, Investigation of the hydration of nonfouling material poly (ethylene glycol) by low-field nuclear magnetic resonance, Langmuir 28 (2012) 2137–2144.
[34] Y.C. Jean, J.D. Van Horn, W.-S. Hung, K.-R. Lee, Perspective of positron annihilation spectroscopy in polymers, Macromolecules 46 (2013) 7133–7145.
[35] K.T. Cao, Z.Y. Jiang, J. Zhao, C.H. Zhao, C.Y. Gao, F.S. Pan, B.Y. Wang, X.Z. Cao, J. Yang, Enhanced water permeation through sodium alginate membranes by incorporating graphene oxides, J. Membr. Sci. 469 (2014) 272–283.
[36] F.B. Peng, L.Y. Lu, C.L. Hu, H. Wu, Z.Y. Jiang, Significant increase of permeation flux and selectivity of poly(vinyl alcohol) membranes by incorporation of crystalline flake graphite, J. Membr. Sci. 259 (2005) 65–73.
[37] J. Zhao, F. Wang, F.S. Pan, M.X. Zhang, X.Y. Yang, P. Li, Z.Y. Jiang, P. Zhang, X.Z. Cao, B.Y. Wang, Enhanced pervaporation dehydration performance of ultrathin hybrid membrane by incorporating bioinspired multifunctional modifier and TiCl4 into chitosan, J. Membr. Sci. 446 (2013) 395–404.
[38] K.T. Cao, Z.Y. Jiang, X.S. Zhang, Y.M. Zhang, J. Zhao, R.S. Xing, S. Yang, C.Y. Gao, F.S. Pan, Highly water-selective hybrid membrane by incorporating g-C3N4 nanosheets into polymer matrix, J. Membr. Sci. 490 (2015) 72–83.
[39] R.S. Xing, F.S. Pan, J. Zhao, K.T. Cao, C.Y. Gao, S. Yang, G.H. Liu, H. Wu, Z.Y. Jiang, Enhancing the permeation selectivity of sodium alginate membrane by incorporating attapulgite nanorods for ethanol dehydration, RSC Adv. 6 (2016) 14381–14392.
[40] B. Gao, Z. Jiang, G. Liu, R. Xing, H. Wu, F. Pan, B. Wang, X. Cao, Enhanced pervaporative performance of hybrid membrane by incorporating amphiphilic carbonaceous material, J. Membr. Sci. 520 (2016) 951–963.
[41] J.A. Wu, Q. Ge, P.T. Mather, PEG-POSS multiblock polyurethanes: synthesis, characterization, and hydrogel formation, Macromolecules 43 (2010) 7637–7649.
[42] A. Kumar, Y. Lee, D. Kim, K.M. Rao, J. Kim, S. Park, A. Haider, D.H. Lee, S.S. Han, Effect of crosslinking functionality on microstructure, mechanical properties, and in vitro cytocompatibility of cellulose nanocrystals reinforced poly (vinyl alcohol)/ sodium alginate hybrid scaffolds, Int. J. Biol. Macromol. 95 (2017) 962–973.
[43] J. Zdarta, M. Wysokowski, M. Norman, A. Kołodziejczak-Radzimska, D. Moszyński, H. Maciejewski, H. Ehrlich, T. Jesionowski, Candida antarctica Lipase B immobilized onto chitin conjugated with POSS(®) compounds: useful tool for rapeseed oil conversion, Int. J. Mol. Sci. 17 (2016) 1581.
[44] E. Markovic, J. Matisons, M. Hussain, G.P. Simon, Poly(ethylene glycol) octafunctionalized polyhedral oligomeric silsesquioxane: waxd and rheological studies, Macromolecules 40 (2007) 4530–4534.
[45] N.L. Le, Y.P. Tang, T.S. Chung, The development of high-performance 6FDA-NDA/ DABA/POSS/Ultem (R) dual-layer hollow fibers for ethanol dehydration via pervaporation, J. Membr. Sci. 447 (2013) 163–176.
[46] A.R. Polu, H.W. Rhee, Nanocomposite solid polymer electrolytes based on poly (ethylene oxide)/POSS-PEG (n=13.3) hybrid nanoparticles for lithium ion batteries, J. Ind. Eng. Chem. 31 (2015) 323–329.
[47] T. Pawlak, A. Kowalewska, B. Zgardzinska, M.J. Potrzebowski, Structure, dynamics, and host-guest interactions in POSS functionalized cross-linked nanoporous hybrid organic-inorganic polymers, J. Phys. Chem. C 119 (2015) 26575–26587.
[48] A. Kudasheva, S. Sorribas, B. Zornoza, C. Tellez, J. Coronas, Pervaporation of water/ethanol mixtures through polyimide based mixed matrix membranes containing ZIF-8, ordered mesoporous silica and ZIF-8-silica core-shell spheres, J. Chem. Technol. Biotechnol. 90 (2015) 669–677.
[49] E.J. Flynn, D.A. Keane, P.M. Tabari, M.A. Morris, Pervaporation performance enhancement through the incorporation of mesoporous silica spheres into PVA membranes, Sep. Purif. Technol. 118 (2013) 73–80.